Thermodynamic Modeling and Experimental Investigation of the System Fe-Ti-O-K for Ilmenite Used as Fluidized Bed Oxygen Carrier

Citation for the original published paper (version of record):
Faust, R., Stanicic, I., Gastaldi, J. et al (2024). Thermodynamic Modeling and Experimental Investigation of the System Fe-Ti-O-K for Ilmenite Used as Fluidized Bed Oxygen Carrier. Energy & Fuels, In Press.
http://dx.doi.org/10.1021/acs.energyfuels.4c02016

(article starts on next page)

energy&fuels

pubs.acs.org/EF
Article

Thermodynamic Modeling and Experimental Investigation of the System Fe−Ti−O-K for Ilmenite Used as Fluidized Bed Oxygen Carrier

Robin Faust,* Ivana Staničić, Jonatan Gastaldi, Elham Ansari, Joakim Brorsson, Tobias Mattisson, Magnus Rydén, and Pavleta Knutsson

Cite This: https://doi.org/10.1021/acs.energyfuels.4c02016
Read Online

ABSTRACT: The capability of ilmenite for potassium uptake in a simulated oxygen carrier-aided combustion environment has been investigated. The maximum uptake of potassium and the effect of potassium inclusion on the Fe−Ti−O system was analyzed. Through laboratory experiments and thermodynamic calculations, it was found that a molar ratio of 1:1 can be formed spontaneously for both the K−Ti-system (where the formation of $K_2Ti_2O_5$ was found) and the K−Fe-system (where $KFeO_2$ was found). $K_2Ti_2O_5$ was identified as an unstable phase, undergoing decomposition into $K_2Ti_4O_9$. The study demonstrates that the maximum K uptake, through forming $K_2Ti_4O_9$ and $KFeO_2$, reaches 25 wt %—a notably higher value than ilmenite exposed to biomass in a fluidized bed. The research concludes that the lifetime of ilmenite is therefore rather dependent on its mechanical integrity than its maximum potassium uptake.

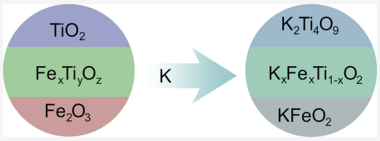

■ BACKGROUND

Oxygen Carrier Aided Combustion (OCAC) is a fluidized bed combustion technology where an Oxygen Carrier (OC) is used as bed material. In addition to the distribution of heat inside the fluidized bed reactor, OCs enhance the distribution of oxygen. This is achieved by undergoing oxidation at high oxygen partial pressures in the reactor and subsequently providing the oxygen at oxygen-lean locations. Therefore, OCAC requires less additional air supply compared to fluidized bed combustion where the bed material is not an OC which increases the efficiency of OCAC.

Oxygen carriers represent materials containing oxides of transition metals that, through continuous oxidation and reduction processes, can transport oxygen in fluidized bed applications. Different materials have been investigated as OCs, for example, the oxides of nickel, copper, iron, manganese, and mixtures thereof.[1] While showing promising results for the combustion process, the limiting factor for these materials has been either the availability, the price, the environmental viability, or the mechanical strength. Therefore, minerals or waste streams containing oxides of transition metals have become the materials of choice for multiple studies using OCs.[2] Several previous publications have covered the existing knowledge of minerals used as oxygen carriers. Among the tested minerals, ilmenite ($FeTiO_3$) is the mineral that has been most widely studied and the only mineral that has been applied in OCAC at an industrial scale.[3,4]

Apart from fulfilling the enumerated criteria for oxygen carrier, ilmenite has also been observed to possess another important feature, which is to capture potassium compounds released during fuel conversion.[5−7] In biomass-based fuels, potassium is one of the major ash compounds. At high temperatures, present in the combustion reactor, potassium compounds can be found both as solid ash or as gaseous KOH or KCl.[8] When K interacts with the bed material or with the available downstream surfaces, the bed material may become sticky, resulting in the formation of deposits, resulting in corrosion, and bed material agglomeration.[9] Thus, the property of ilmenite to capture potassium can decrease the risk of corrosion and agglomeration and lead to fewer unplanned plant stops and lower material consumption. To optimize the combustion process when it comes to the uptake of potassium by ilmenite, a clear understanding of the interactions of potassium with the bed material and the resulting compounds is needed.

Multiple studies have been performed on the interactions of ilmenite with potassium originating from the formed ash by ex situ analysis of solid material. According to most of these studies, iron from ilmenite diffuses outward to the surface of the oxygen carrier forming an iron oxide layer,[4,5,10] while potassium migrates inward to the segregated Ti-enriched phase of the oxygen-carrying particles, forming potassium titanates.[5] As a result of the potassium migration and interactions, several potassium titanates have been mentioned as possible products

Received: April 29, 2024
Revised: July 10, 2024
Accepted: July 10, 2024

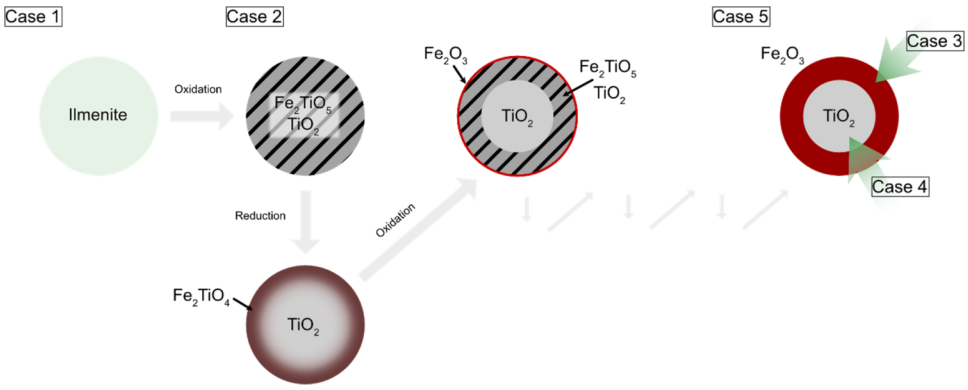

Figure 1. Schematic depiction of the development of the distribution of Fe and Ti in ilmenite over time. The different cases considered in this study are indicated.

Table 1. Elemental Composition of the Ilmenite Used for This Study[a]

Fe	Ti	Mn	Mg	Al	Si	K	Ca	Na	P	Ba
47.5	43.0	0.3	6.1	0.5	1.8	0.1	0.4	0.3	0.1	0.1

[a]Values are shown in atom % on an O-free basis.

in the performed studies − $K_{0.4}Fe_{0.4}Ti_{0.6}O_2$, $K_{0.85}Fe_{0.85}Ti_{0.15}O_2$, and different priderites[11] with the general formula $K_xTi_{8-x}(Fe^{3+},Ti^{3+})_xO_{16}$ which comprises KTi_8O_{16},[5,12,13] and $K_{1.5}Ti_{7.2}Fe_{0.8}O_{16}$.[4] In the published investigations the uptake of potassium has been measured and the obtained values vary from 2−4 wt %[5,6,14] and up to 10 wt %.[13] From thermodynamic calculations conducted for the interactions of K_2O with ilmenite, $K_2Ti_6O_{13}$ is commonly found as the most stable product,[13,15,16] while studies using phase analysis with X-ray diffraction (XRD) usually find the formation of priderite.[4,5,11−13] Even though the existing studies provide a certain understanding of the mechanism of potassium diffusion, they do not provide the mechanism behind the formation of different titanates which could explain the different observed uptake mechanisms of potassium by ilmenite. Understanding potassium diffusion and interactions, as well as predicting maximum potassium uptake is crucial to decide the residence time of the material in the plant and to plan for optimal operational conditions and rate of replacement of bed material.

Fresh ilmenite consists mainly of $FeTiO_3$. During its utilization as an oxygen carrier, the ilmenite particles undergo several changes. Under oxidizing conditions, ilmenite is oxidized to pseudobrookite (Fe_2TiO_5) and rutile (TiO_2) according to Reaction 1. At reducing conditions, pseudobrookite can be reduced to ulvöspinel (Fe_2TiO_4), thereby releasing O_2 available to contribute to fuel conversion, Reaction 2.[17] Ulvöspinel in the surface vicinity will subsequently be oxidized to hematite at oxidizing conditions, shown in Reaction 3, and thereby contributes to the oxygen-carrying effect of the bed material.

$$2FeTiO_3 + 1/2O_2 \rightarrow Fe_2TiO_5 + TiO_2 \quad (1)$$

$$Fe_2TiO_5 \rightarrow Fe_2TiO_4 + 1/2O_2 \quad (2)$$

$$Fe_2TiO_4 + 1/2O_2 \rightarrow Fe_2O_3 + TiO_2 \quad (3)$$

Through this process, a gradual migration of iron to the surface of the particles has been observed by multiple studies on ilmenite used for fluidized bed applications.[6,10,18,19] Outward diffusion of iron increases the metal available for oxygen carrying and thereby increases the fuel conversion. Analysis of particles exposed to alternating oxidizing and reducing atmospheres has confirmed the presence of a thin layer of iron on the surface, increasing in thickness with time, which was identified as Fe_2O_3. The formation of Fe_2O_3 leaves behind an increased concentration of TiO_2 in the core of the particles. Continuous oxidation and reduction results thus in a gradient of phases decreasing in Fe-content and increasing in Ti content which follows five main cases schematically shown in Figure 1 and described as follows:

- Case 1 in the figure represents the fresh ilmenite particles prior to their utilization.
- Case 2 represents the ilmenite particles after oxidation where the two phases pseudobrookite (Fe_2TiO_5) and rutile (TiO_2) are present.
- Case 3 represents the layer of Fe_2O_3 which gradually forms on the surface after several oxidation/reduction cycles.
- Case 4 represents the TiO_2-rich core of used ilmenite particles which is exposed after the Fe-rich layer is removed through attrition.
- Case 5 represents the mixture of Fe_2O_3 and TiO_2 to be equally accessible when utilizing ilmenite as an oxygen carrier.

Each of these stages can result in different interaction pathways for the inward migrating potassium and will therefore lead to a different maximum uptake of potassium and a different lifetime of ilmenite used as bed material. The five main interaction cases can be highly relevant to the different uptake mechanisms of potassium that are presented in the literature. To understand the significance of each of the mentioned stages for the interaction with the potassium, model systems isolating each case need to be used. The present work aims to determine the maximum potassium uptake under laboratory conditions and by thermodynamic modeling, which has not been done before. By decoupling different stages of development and investigating isolated cases as illustrated in Figure 1, a deeper understanding can be obtained of the Fe−Ti−O-K system, which can then be used to predict potassium

https://doi.org/10.1021/acs.energyfuels.4c02016
Energy Fuels XXXX, XXX, XXX−XXX

interactions under different process conditions. At a later stage, this knowledge can be applied to better understand and predict the lifetime of bed material in the reactor.

■ MATERIALS AND METHODS

To obtain a better understanding, dedicated experiments of ilmenite-alkali experiments were conducted. Here, solid-state interactions were applied, as this is believed to give a valid view of chemical phenomena. The ilmenite used for the experiments was obtained from Titania A/S from Norway. The elemental composition is shown in Table 1. Ilmenite was used as particles with a particle size of 180−710 μm. The other chemicals were provided as a powder, Fe_2O_3 (97% pure, Riedel-de Haën), TiO_2 (>99%, Merck), and K_2CO_3 (>99%, Alfa Aesar).

Experimental Setup. Exposures were conducted to investigate the mechanism of potassium uptake by the different phases present in ilmenite particles during their utilization as an oxygen carrier.

K_2CO_3 was selected as a source of reactive potassium. The exposures were conducted in ambient air and the temperature was set to 1000 °C which represents the expected temperatures for optimal fluidized bed combustion processes. The K interactions with materials from different cases were mimicked by mixing K_2CO_3 with the selected sample as powders inside an alumina crucible. Two parameters were investigated for each of the five cases, namely the effect of exposure time and the effect of additional K addition. For experiments investigating the effect of exposure time, the molar ratio of model oxygen carrier to potassium was chosen to be 2:1. The second investigated parameter was the effect of oversaturation of the K−Ti−O system with K to evaluate the theoretic maximum uptake of K by the particles. For these exposures, two additional doses of K_2CO_3 were added to the crucible after 24 and 48 h, changing the molar ratio of the model oxygen carrier to potassium to 2:3. The addition was done by removing the crucible from the furnace and the salt was added after about five minutes. This continuous addition was performed to simulate the conditions present in a fluidized bed reactor, where fuel ash is continuously added to the bed material. The results were compared to a reference exposure where no K_2CO_3 was added. The reference exposure was conducted for 7 days without the addition of K_2CO_3. Table 2 provides a summary of the 20 samples that were investigated in this study and introduces the abbreviations that will be used during the results and discussion.

X-ray Diffraction. After the exposures, the samples were investigated with X-ray diffraction (XRD) with a Bruker D8 Discover. Prior to the analysis, the samples were ground to a fine powder and mounted on a Zero-background sample holder. Mo Kα radiation (λ = 0.70930 Å) was used for the samples containing Fe (cases 1, 2, 3, and 5) to minimize high background due to sample fluorescence. The samples containing only TiO_2 and K_2CO_3 (case 4) were analyzed with the commonly used Cu Kα radiation (λ = 1.5406 Å). The acquired diffraction patterns were compared to the PDF 2022 database. Semiquantitative analysis taking the relative intensities of the peaks of the different identified phases into consideration was done to obtain information on the relative amounts of the phases.

Thermodynamic Modeling. Thermodynamic calculations were performed using the software FactSage 8.2 and the module *Equilib*.[20] Thermodynamic calculations determine the chemical equilibrium by minimizing Gibbs free energy considering thermodynamic data for various phases and compounds. In this work, the database for pure substances (FactPS), oxide solutions (FToxid), and relevant compounds from other sources were integrated with a user-defined database and utilized along with additional thermal data for compounds previously shown to be important within the potassium−oxygen carrier systems namely, KTi_8O_{16} and $K_xFe_xTi_{1-x}O_2$ where x = 0.85 or 0.4.[21] In case of conflicting data, priority was given to FToxid, FactPS and last the user-defined database.

The calculations were carried out using the *Equilib* module under conditions identical to those of the experiments (1000 °C and oxidizing conditions using air) with the aim of obtaining a better understanding of the phase transitions in the system. The *Reaction* module was used to study in more detail. Lastly, the module *Phase Diagram* was utilized to generate phase diagrams for the K−Fe−Ti−O system to provide a better view of how variations in concentration within the sample can impact the results. The following solution phases were selected in the calculations; spinel, monoxide, corundum, rutile, ilmenite, pseudobrookite, and titania spinel. Considering that there was no indication of the formation of molten phases during exposures, the molten solution phase was not included in the model.

Table 2. Summary of the Time and Exposed Materials[a]

	Fe−Ti−O	time (days)	molar ratio (Fe−Ti)/K	abbreviation
case 1	ilmenite	1	2:1	Ilm1d
	ilmenite	7	2:1	Ilm7d
	ilmenite	3	2:3	Ilm3K
	ilmenite	7		IlmR
case 2	calcined ilmenite	1	2:1	cIlm1d
	calcined ilmenite	7	2:1	cIlm7d
	Calcined ilmenite	3	2:3	cIlm3K
	calcined ilmenite	7		cIlmR
case 3	Fe_2O_3	1	2:1	Hem1d
	Fe_2O_3	7	2:1	Hem7d
	Fe_2O_3	3	2:3	Hem3K
	Fe_2O_3	7		HemR
case 4	TiO_2	1	2:1	Rut1d
	TiO_2	7	2:1	Rut7d
	TiO_2	3	2:3	Rut3K
	TiO_2	7		RutR
case 5	Fe_2O_3/TiO_2	1	2:1	HeRu 1d
	Fe_2O_3/TiO_2	7	2:1	HeRu7d
	Fe_2O_3/TiO_2	3	2:3	HeRu3K
	Fe_2O_3/TiO_2	7		HeRuR

[a]Cases 1 and 2 were done with mineral particles of ilmenite before and after calcination respectively. Cases 3, 4, and 5 were done with pure chemicals. Exposure conditions for all set-ups were done in air at 1000 °C.

While available thermodynamic databases provide data for a wide range of materials there are materials and phases which are missing from databases. In these cases, it is possible to expand the thermodynamic database using first-principles calculations. The method used in this article has been published separately,[15] and entails computing the reaction energies by using density functional theory (DFT) and calculating the phononic contribution to the heat capacity using harmonic approximation. Using the procedure presented by Benisek and Dachs,[22] the results from the first-principles calculations were combined with experimental data from NIST-JANAF thermochemical tables. This combination makes it possible to determine the enthalpy and entropy at room temperature as well as the temperature dependence of the heat capacity. The method has been used previously and provided results in excellent agreement with experimental data for other iron-oxides, especially $FeTiO_3$.[15,16]

FactSage requires that the temperature dependence of the specific heat capacity is provided as the sum of power functions

$$C_p(T) = \sum_{i=1}^{8} k_i T^{p_i} \tag{4}$$

Most materials in FactSage use an expression of the specific heat capacity with four terms, which has also been employed in this study.

$$C_p(T) = k_1 + k_2 T^{-2} + k_3 T^{-0.5} + k_4 T^{-3} \tag{5}$$

■ RESULTS

Experimental Results. All the exposed samples were characterized by XRD to identify the formed phases. The

https://doi.org/10.1021/acs.energyfuels.4c02016
Energy Fuels XXXX, XXX, XXX−XXX

Table 3. Composition of the Samples after Exposure Based on Semi-Quantitative XRD Results (Results Shown in mol %)

		hematite	$K_xFe_xTi_{1-x}O_2$ (x = 0.4)	$K_xFe_xTi_{1-x}O_2$ (x = 0.85)	TiO_2	$K_xTi_{8-x}(Fe,Ti)_xO_{16}$ (priderite)	$K_2Ti_6O_{13}$	$K_3Ti_8O_{17}$	$K_2Ti_4O_9$	$K_2Ti_2O_5$	$KFe_{11}O_{17}$	$KFeO_2$	Fe_2TiO_5
case 1	Ilm1d	49	37			15							
	Ilm7d	32	57			11							
	Ilm3K		55	45									
	IlmR				16								84
case 2	cIlm1d	16	75				8						
	cIlm7d	21	71				8						
	cIlm3K		17	83									
	cIlmR				12								88
case 3	Hem1d	20									4	76	
	Hem7d	21									14	65	
	Hem3K											100	
	HemR	100											
case 4	Rut1d				26		8		23	43			
	Rut7d				49		20		31				
	Rut3K				11					89			
	RutR				100								
case 5	HeRu 1d	56	32					12					
	HeRu7d	43	27			20		10					
	HeRu3K		27	73									
	HeRuR	44			49								7

https://doi.org/10.1021/acs.energyfuels.4c02016
Energy Fuels XXXX, XXX, XXX−XXX

Table 4. Thermodynamic Properties at 298.15 K[a]

compound	$\Delta_f H$ (J/mol)	S (J/(molK)	k_1 (J/(molK))	k_2 (JK/mol)	k_3 (J/(molK$^{0.5}$))	k_4 (JK^2/mol)
$KFe_{11}O_{17}$	-4.87×10^6	570.88	553.14	-1.48×10^8	13,820.07	2.38×10^{10}
$K_2Fe_{10}O_{16}$	-2.15×10^6	249.43	321.33	-5.76×10^7	4600.90	9.05×10^9

[a]The formation enthalpy, entropy, and coefficients in the expression for heat capacity, eq 5, are listed for the two compounds $KFe_{11}O_{17}$ and $K_2Fe_{10}O_{16}$.

Table 5. Phases Formed at Equilibrium for Each Exposure[a]

system	case	$\frac{Fe-Ti}{K}$	predicted phases	observed phases	exposure
K−Fe−Ti	1	2:1	$\mathbf{K_2Ti_6O_{13}}$ + $K_2Ti_3O_7$ + $KFe_{11}O_{17}$	priderite + $K_{0.4}Fe_{0.4}Ti_{0.6}O_2$	Ilm1d, Ilm7d
	2			$\mathbf{K_2Ti_6O_{13}}$ + $K_{0.4}Fe_{0.4}Ti_{0.6}O_2$	cIlm1d, cIlm7d
K−Fe−Ti	1 + 2	2:3	$K_8Ti_5O_{14}$ + $K_2Ti_2O_5$ + $KFe_{11}O_{17}$	$K_{0.4}Fe_{0.4}Ti_{0.6}O_2$ + $K_{0.85}Fe_{0.85}Ti_{0.15}O_2$	Ilm3K, cIlm3K
K−Fe	3	2:1	$\mathbf{KFeO_2}$ + $\mathbf{KFe_{11}O_{17}}$	$\mathbf{KFe_{11}O_{17}}$ + $\mathbf{KFeO_2}$	Hem1d, Hem7d
K−Fe	3	2:3	$\mathbf{KFeO_2}$	$KFe_{11}O_{17}$ + $\mathbf{KFeO_2}$	Hem3K
K−Ti	4	2:1	$\mathbf{K_2Ti_6O_{13}}$ + $K_2Ti_3O_7$	$\mathbf{K_2Ti_6O_{13}}$ + $K_2Ti_4O_9$ + $K_2Ti_2O_5$ (Rut1d)	Rut1d, Rut7d
K−Ti	4	2:3	$\mathbf{K_2Ti_2O_5}$ + $K_8Ti_5O_{14}$	$\mathbf{K_2Ti_2O_5}$	Rut3K
K−Fe−Ti	5	2:1	$K_2Ti_6O_{13}$ + $K_2Ti_3O_{7+}$ + $KFe_{11}O_{17}$	$K_3Ti_8O_{17}$ + $K_{0.4}Fe_{0.4}Ti_{0.6}O_2$ + priderite (HeRu7d)	HeRu 1d, HeRu7d
K−Fe−Ti	5	2:3	$K_8Ti_5O_{14}$ + $K_2Ti_2O_{5+}$ + $KFe_{11}O_{17}$	$K_{0.4}Fe_{0.4}Ti_{0.6}O_2$ + $K_{0.85}Fe_{0.85}$ $Ti_{0.15}O_2$	HeRu3K

[a]Phases that form due to interaction, that are both predicted and observed, are presented in bold.

results of XRD are shown in Table 3. The peak intensities of the matched phases were used to assign semiquantitative values to estimate the respective amount of each phase in the sample.

Case 1 describes the interaction between fresh ilmenite particles and K_2CO_3. As expected, the reference case IlmR (without the addition of K_2CO_3) contains Fe_2TiO_5 and TiO_2 which are formed through the oxidation of ilmenite as shown in Reaction 1. The amount of Fe_2TiO_5 was higher than the theoretical value of 50% that is obtained through the reaction, which can be explained by the pseudobrookite solid solution extending between a cationic content of 30 and 70% of Fe (with between 70 and 30% Ti accordingly).[17,23] The addition of K_2CO_3 to ilmenite in this case leads to the disappearance of pseudobrookite through the reaction of Ti with K to priderite ($K_xTi_{8-x}(Fe^{3+},Ti^{3+})_xO_{16}$) and $K_{0.4}Fe_{0.4}Ti_{0.6}O_2$ (Ilm1d and Ilm7d). This leaves the remaining Fe as Fe_2O_3 due to the lack of a reaction partner, which is why it was found as a separate phase. Increasing the amount of K available for reaction (Ilm3K) yields $K_{0.4}Fe_{0.4}Ti_{0.6}O_2$ and $K_{0.85}Fe_{0.85}Ti_{0.15}O_2$ as stable phases. This suggests that if there is a sufficient K amount and Fe_2O_3 is available for reaction, mixed K−Fe−Ti-oxides will form that are more stable than K-titanates which are commonly observed when studying ilmenite interactions with biomass ash.[5,12,13]

Similar observations were made in **Case 2**, where ilmenite was calcined before the exposure to K_2CO_3. XRD results suggest that the interaction between calcined ilmenite and K_2CO_3 proceeds further than with fresh ilmenite, as the relative share of interaction products is larger than with fresh ilmenite. Furthermore, $K_2Ti_6O_{13}$ is found in Case 2 at 2:1 concentrations of K_2CO_3 (cIlm1d and cIlm7d) which is the K-titanate that is expected to form at equilibrium.[13,16]

Case 3 describes the reaction that is expected to take place on the surface of ilmenite particles which have been activated by several redox cycles and have thereby formed a Fe_2O_3 (hematite) rich surface layer. At lower K_2CO_3 additions (Hem1d and Hem7d), the main product of the reaction is $KFeO_2$, with small amounts of $KFe_{11}O_{17}$ and approximately 20% unreacted Fe_2O_3. This indicates that the possible uptake of K by ilmenite is not only dependent on the availability of TiO_2, but it can also form stable compounds with available Fe_2O_3. Adding further K_2CO_3 to Fe_2O_3 (Hem3K) yields 100% $KFeO_2$ as a final product which shows the maximum of K that can be taken up by Fe_2O_3.

Case 4 explores the reactions that occur with TiO_2 (rutile) and K_2CO_3 without the presence of Fe in the system. Lower additions of K_2CO_3 to rutile and an interaction time of 24 h (Rut1d) lead to the formation of three different K-titanates with different ratios of K:Ti. The highest ratio is reached in $K_2Ti_2O_5$ indicating that this phase represents the highest possible amount of K which can be taken up by TiO_2. However, increasing the interaction time to 7 days causes the disappearance of this phase in favor of titanates containing lower ratios of K/Ti. This suggests a lack of stability of $K_2Ti_2O_5$ and indicates a K release from $K_2Ti_2O_5$, most likely as $KOH_{(g)}$. Continuous addition of K_2CO_3 to the system (Rut3K) stabilizes this phase, and it becomes almost the only detectable phase.

Case 5 investigates the interactions between Fe_2O_3 (hematite), TiO_2 (rutile), and K_2CO_3, which represents the case of complete phase-separated ilmenite. The interaction is similar to Cases 1 and 2, where the addition of small amounts of K_2CO_3 (HeRu 1d and HeRu7d) leads to the formation of $K_{0.4}Fe_{0.4}Ti_{0.6}O_2$, while after the addition of three times as much (HeRu3K), $K_{0.85}Fe_{0.85}Ti_{0.15}O_2$ is formed. The only difference is observed in the K-titanates which are detected. $K_3Ti_8O_{17}$ is detected in this case while priderite is only found after 7 days of interaction time (HeRu7d).

Modeling. *Database Expansion.* Correlating the experimental observation with the initial thermodynamic model showed that the phases $K_3Ti_8O_{17}$, $K_2Ti_4O_9$, $KFe_{11}O_{17}$, and $K_2Fe_{10}O_{16}$ did not have thermodynamic entries in the available databases, meaning that the model could not account for these compounds. Consequently, thermal data was derived from first-principles calculations and incorporated into the user-defined database. The selected compounds were $KFe_{11}O_{17}$ and $K_2Fe_{10}O_{16}$, and they were selected as it was difficult to distinguish them in the diffractogram.

The estimations of thermodynamic properties of the interesting phases are dependent on the thermodynamic data of known binary oxides which was used as reference together

https://doi.org/10.1021/acs.energyfuels.4c02016
Energy Fuels XXXX, XXX, XXX−XXX

with the results of the first-principles calculations. Fe_2O_3 and K_2O were deemed to be the best fit as reference materials which made the following reactions the most suitable for each system

$$5.5Fe_2O_3 + 0.5K_2O \rightleftharpoons KFe_{11}O_{17} \quad (6)$$

$$5Fe_2O_3 + K_2O \rightleftharpoons K_2Fe_{10}O_{16} \quad (7)$$

The thermodynamic data of Fe_2O_3 and K_2O was taken from NIST-JANAF. The thermodynamic properties and constants used in eq 5 for $KFe_{11}O_{17}$ and $K_2Fe_{10}O_{16}$ are shown in Table 4.

Thermodynamic Model. The thermodynamic phase stability for each exposure was investigated in air at 1000 °C. The anticipated phases after exposures are outlined in Table 5. Additionally, since the calculations are independent of time and are solely based on the molar ratio between the components, the findings in Table 5 can be valid across multiple exposures. Given that the temperature, gaseous conditions, and molar ratio in the K−Fe−Ti-O systems were similar across the exposures, it is anticipated that these systems will eventually reach the same equilibrium state.

The ternary phase diagram for Fe_2O_3−TiO_2−K_2CO_3 in air, at 1 atm and 1000 °C, is presented in Figure 2. The phase diagram was constructed to present all possible transformations within the K−Fe−Ti−O system. A small amount of moisture (p_{H2O} = 0.01 atm) was included to account for the possible presence of KOH. It was observed that moisture promoted the formation of KOH. The carbon from K_2CO_3 is present as CO_2 across the whole diagram. The experimental conditions are illustrated in Figure 2 with filled and half-filled symbols representing different loadings of K_2CO_3. Due to the homogeneous composition of Fe−Ti−O in cases 1, 2, and 5, the thermodynamic outcome is identical. For these systems, it can be observed that the presence of K_2CO_3 facilitates the separation of Fe and Ti, due to the formation of K-titanates and K-ferrites.

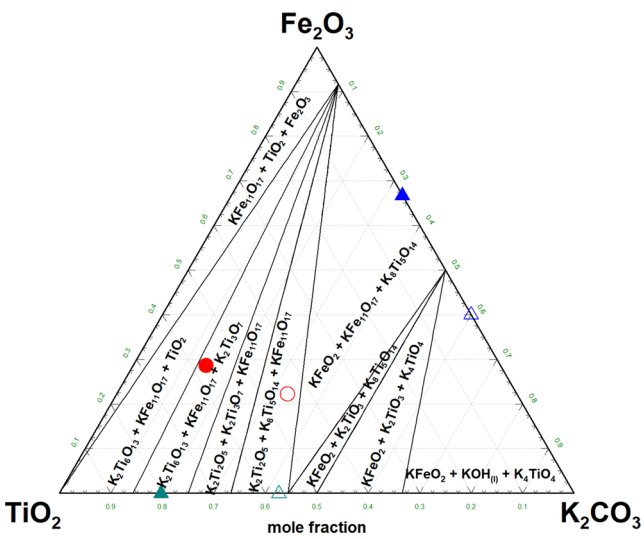

Figure 2. Ternary phase diagram of Fe_2O_3−TiO_2−K_2CO_3 in air, with 0.1% moisture, at 1000 °C, and 1 atm. Experimental conditions representing the ratio [Fe-T]/K = 2:1 and 2:3 are indicated by the filled and half-filled symbols, respectively. The red, blue, and green colors symbolize experiments within the systems K−Fe−Ti, K−Fe, and K−Ti, respectively.

The introduction of the new data set improved the predictability of K−Fe-based systems. For example, evident from Table 3 is that thermodynamic equilibrium is reached in cases 3 and 4 since the experimental observations for the systems K−Fe and K−Ti are well aligned with the equilibrium phases. However, even with the provided data for compounds such as KTi_8O_{16} and $K_xFe_xTi_{1-x}O_2$ (x = 0.85 or 0.4), these phases did not form under equilibrium conditions within the specified systems. A more in-depth investigation was conducted to elucidate the behavior of these specific phases. The Gibbs free energy for shows that the reactions forming KTi_8O_{16} and $K_xFe_xTi_{1-x}O_2$ are spontaneous. It is thus probable that when these compounds form, they can prevent the formation of equilibrium phases due to limitations in mixing.

$$0.2K_2O_{(s)} + 0.2Fe_2O_{3(s)} + 0.6TiO_{2(s)} \rightarrow K_{0.4}Fe_{0.4}Ti_{0.6}O_{2(s)} \quad \Delta G\ (1000\ ^\circ C) = -61.3\ kJ \quad (8)$$

$$0.425K_2O_{(s)} + 0.425Fe_2O_{3(s)} + 0.15TiO_{2(s)} \rightarrow K_{0.85}Fe_{0.85}Ti_{0.15}O_{2(s)} \quad \Delta G\ (1000\ ^\circ C) = -60.6\ kJ \quad (9)$$

$$2K_2O_{(s)} + 32TiO_{2(s)} \rightarrow 4KTi_8O_{16(s)} + O_{2(g)} \quad \Delta G\ (1000\ ^\circ C) = -418.5\ kJ \quad (10)$$

Looking at the stability of K−Ti-phases it is observed that increasing the amount of K_2CO_3 to the system leads to an increase in the K/Ti-ratio. The evolution of phases is as follows; $K_2Ti_6O_{13}$−$K_2Ti_3O_7$−$K_2Ti_2O_5$−$K_8Ti_5O_{14}$−K_2TiO_3−K_4TiO_4, where the K/Ti ratio increases from 0.33 to 4. The highest K/Ti-ratio is achieved in K_4TiO_4, which forms when the concentration of K_2CO_3 exceeds 50 atom %. However, these conditions are not reached during biomass conversion. A more likely scenario is in the region where the phase $K_2Ti_2O_5$ is experimentally observed. The phase $K_2Ti_3O_7$ could provide a higher capability for potassium uptake, but unfortunately, $K_2Ti_2O_5$ is not stable with a longer increasing exposure time. Therefore, the phase with the highest stability and maximum potassium uptake is $K_2Ti_6O_{13}$.

■ DISCUSSION

In the current study, K−Fe−Ti−O systems were selected to follow the maximum potassium uptake by isolating different stages during the lifetime of ilmenite. Both model system compounds exposed in laboratory conditions and thermodynamic modeling studies were used to follow the possible interactions. This allowed for a systematic investigation of the K−Fe−Ti−O system. Ilmenite was used as a system boundary defining conditions and the selected model compounds were based on phases observed to form during continuous redox cycles. The study shows that potassium will preferably interact with titanium in systems that contain iron and titanium oxides. Experiments consistently reveal the interaction between K_2CO_3 and TiO_2 is favored over the reaction with Fe_2O_3. The detected phases in laboratory tests are further supported by modeling. In cases where both hematite and rutile are available, the reaction products at low K concentrations are

https://doi.org/10.1021/acs.energyfuels.4c02016
Energy Fuels XXXX, XXX, XXX−XXX

different K-titanates and $K_{0.4}Fe_{0.4}Ti_{0.6}O_2$ with around 20−50% hematite remaining. Only after further addition of K to the system is the hematite consumed in favor of the formation of $K_{0.85}Fe_{0.85}Ti_{0.15}O_2$.

Calcined ilmenite, Case 2, represents particles after oxidation where both pseudobrookite (Fe_2TiO_5) and rutile (TiO_2) are present. Interestingly, calcined ilmenite forms $K_2Ti_6O_{13}$ instead of the commonly observed priderite, which was found to form during the exposure of fresh ilmenite.[5,6,13] This could be an indication that the outward migration of Fe which occurs during calcination inhibits the formation of priderite. This agrees with the fact that in industrial applications, the ilmenite particles are usually not precalcined, and priderite is commonly observed.[5] It also means that through the segregation of Fe_2O_3 by its migration to the surface allows for a higher uptake of K by TiO_2 to form $K_2Ti_6O_{13}$. This suggests that with increasing exposure time, ilmenite would form $K_2Ti_6O_{13}$ if a continuous flow of K is provided. However, this phase is not found during XRD analysis of ilmenite particles that have interacted with K-rich biomass. An important difference between the experiments done in this study compared to biomass ash is the presence of Ca, which forms Ca-rich layers on the surface of ilmenite particles. The Ca-rich layer which is usually observed in these cases contains $CaTiO_3$ and could participate in limiting the supply of additional K toward the Ti-rich core of aged ilmenite particles, inhibiting the formation of $K_2Ti_6O_{13}$.

The spontaneous formation of $KFeO_2$ and $KFe_{11}O_{17}$ occurring in the system representing the surface of aged ilmenite could represent a first step for the interaction of ilmenite with alkali species. This would mean that in a fluidized bed reactor, Fe_2O_3-covered ilmenite particles pick up alkali species through the formation of $KFeO_2$. As the K-titanates are thermodynamically more stable, they are formed through the interaction between $KFeO_2$ and TiO_2.

This study allows several conclusions to be drawn regarding the maximum potential uptake of potassium by ilmenite. Both rutile and hematite spontaneously take up K in a molar ratio of K/Fe and K/Ti of 1:1, as in $KFeO_2$ and $K_2Ti_2O_5$. Although $KFeO_2$ appears to be stable over time, $K_2Ti_2O_5$ seems to dissociate to $K_2Ti_4O_9$ which possibly is associated with the release of gaseous KOH through the reaction with air-derived moisture. Based on the formation of $KFeO_2$ and $K_2Ti_4O_9$, the total maximum uptake of K by ilmenite is therefore 25 wt % (see Reaction 11). However, as mentioned previously, ilmenite particles utilized in fluidized bed applications usually contain significantly lower amounts of K (around 4 wt %) and priderite is commonly observed with XRD. The products of the corresponding Reaction 12 contain around 3 wt % K. Particle fragmentation is commonly observed for ilmenite utilized for prolonged times in fluidized bed applications which is why fresh material is regularly added to the reactors.[4,24] With the results from the current study, it can be concluded that the mechanical properties are more decisive for the maximum lifetime of ilmenite than its capability of K uptake.

$$3K_2O + 4FeTiO_3 + O_2 \rightarrow 4KFeO_2 + K_2Ti_4O_9 \quad (11)$$

$$K_2O + 16FeTiO_3 + 4O_2 \rightarrow 2KTi_8O_{16} + 8Fe_2O_3 \quad (12)$$

CONCLUSIONS

This study explored the interaction between different cases formed during the lifetime of ilmenite used as an oxygen carrier with high concentrations of K_2CO_3. The maximum uptake of K by ilmenite was assessed.

- A molar ratio of 1:1 was found to spontaneously form for both K/Ti ($K_2Ti_2O_5$) and K/Fe ($KFeO_2$). $K_2Ti_2O_5$ was found to be unstable and to decompose to $K_2Ti_4O_9$.
- $KFeO_2$ could be a primary interaction product of the interaction of aged ilmenite with alkali species.
- The maximum uptake of K through the formation of $K_2Ti_4O_9$ and $KFeO_2$ is 25 wt %, which is significantly higher than what is measured for ilmenite exposed to biomass in a fluidized bed.
- The maximum lifetime of ilmenite is dependent on its mechanical properties rather than its total K uptake capacity.

AUTHOR INFORMATION

Corresponding Author

Robin Faust − *Department of Chemistry and Chemical Engineering, Division of Energy Technology, Chalmers University of Technology, SE-412 96 Gothenburg, Sweden;* orcid.org/0000-0001-5614-3578; Email: faust@chalmers.se

Authors

Ivana Staničić − *Department of Space, Earth and Environment, Division of Energy Technology, Chalmers University of Technology, SE-412 96 Gothenburg, Sweden;* orcid.org/0000-0002-6927-4822

Jonatan Gastaldi − *Department of Space, Earth and Environment, Division of Energy Technology, Chalmers University of Technology, SE-412 96 Gothenburg, Sweden*

Elham Ansari − *Department of Chemistry and Chemical Engineering, Division of Energy Technology, Chalmers University of Technology, SE-412 96 Gothenburg, Sweden*

Joakim Brorsson − *Department of Physics, Division of Chemical Physics, Chalmers University of Technology, SE-412 96 Gothenburg, Sweden*

Tobias Mattisson − *Department of Space, Earth and Environment, Division of Energy Technology, Chalmers University of Technology, SE-412 96 Gothenburg, Sweden;* orcid.org/0000-0003-3942-7434

Magnus Rydén − *Department of Space, Earth and Environment, Division of Energy Technology, Chalmers University of Technology, SE-412 96 Gothenburg, Sweden*

Pavleta Knutsson − *Department of Chemistry and Chemical Engineering, Division of Energy Technology, Chalmers University of Technology, SE-412 96 Gothenburg, Sweden*

Complete contact information is available at: https://pubs.acs.org/10.1021/acs.energyfuels.4c02016

Author Contributions

R.F.: Conceptualization, methodology, investigation, writing—original draft, writing—review and editing. I.S.: Methodology, writing − original draft. J.G.: Methodology, formal analysis, writing—original draft. E.A.: Investigation. J.B.: Formal analysis, writing—Review and editing. T.M.: Writing − Review and editing. M.R.: Writing − review and editing. P.K.: Conceptualization, writing − original draft, writing − review and editing.

Notes

The authors declare no competing financial interest.

https://doi.org/10.1021/acs.energyfuels.4c02016
Energy Fuels XXXX, XXX, XXX−XXX

■ ACKNOWLEDGMENTS

The computations were enabled by resources provided by the National Academic Infrastructure for Supercomputing in Sweden (NAISS) at NSC and PDC partially funded by the Swedish Research Council through grant agreement no. 2022-06725.

■ REFERENCES

(1) Lyngfelt, A. Chemical Looping Combustion: Status and Development Challenges. *Energy Fuels* **2020**, *34*, 9077−9093.

(2) Störner, F.; Lind, F.; Rydén, M. Oxygen Carrier Aided Combustion in Fluidized Bed Boilers in Sweden—Review and Future Outlook with Respect to Affordable Bed Materials. *Appl. Sci.* **2021**, *11*, No. 7935, DOI: 10.3390/app11177935.

(3) Andersson, V.; Staničić, I.; Kong, X.; Leion, H.; Mattisson, T.; Pettersson, J. B. C. Alkali desorption from ilmenite oxygen carrier particles used in biomass combustion. *Fuel* **2024**, *359*, No. 130400.

(4) Dieringer, P.; Marx, F.; Lebendig, F.; Müller, M.; Di Giuliano, A.; Gallucci, K.; Ströhle, J.; Epple, B. Fate of ilmenite as oxygen carrier during 1 MWth chemical looping gasification of biogenic residues. *Appl. Energy Combust. Sci.* **2023**, *16*, No. 100227.

(5) Corcoran, A.; Marinkovic, J.; Lind, F.; Thunman, H.; Knutsson, P.; Seemann, M. Ash Properties of Ilmenite Used as Bed Material for Combustion of Biomass in a Circulating Fluidized Bed Boiler. *Energy Fuels* **2014**, *28*, 7672−7679.

(6) Corcoran, A.; Knutsson, P.; Lind, F.; Thunman, H. Mechanism for Migration and Layer Growth of Biomass Ash on Ilmenite Used for Oxygen Carrier Aided Combustion. *Energy Fuels* **2018**, *32*, 8845−8856.

(7) Li, L.; Mao, J.; Tang, W.; Sun, G.; Gu, Q.; Lu, X.; Shao, K.; Chen, Y.; Duan, L. Experimental study on coal combustion by using the ilmenite ore as active bed material in a 0.3 MWth circulating fluidized bed. *Fuel* **2023**, *342*, No. 127007, DOI: 10.1016/j.fuel.2022.127007.

(8) Gogolev, I.; Pikkarainen, T.; Kauppinen, J.; Linderholm, C.; Steenari, B.-M.; Lyngfelt, A. Investigation of biomass alkali release in a dual circulating fluidized bed chemical looping combustion system. *Fuel* **2021**, *297*, No. 120743.

(9) Pettersson, J.; Svensson, J. E.; Johansson, L. G. Alkali Induced Corrosion of 304-Type Austenitic Stainless Steel at 600 °C; Comparison between KCl, K2CO3 and K2SO4. *Mater. Sci. Forum* **2008**, *595−598*, 367−375.

(10) Bartocci, P.; Abad, A.; Mattisson, T.; Cabello, A.; Loscertales, M. D. L. O.; Negredo, T. M.; Zampilli, M.; Taiana, A.; Serra, A.; Arauzo, I.; et al. Bioenergy with Carbon Capture and Storage (BECCS) developed by coupling a Pressurised Chemical Looping combustor with a turbo expander: How to optimize plant efficiency. *Renewable Sustainable Energy Rev.* **2022**, *169*, No. 112851.

(11) Hildor, F.; Yilmaz, D.; Leion, H. Interaction behavior of sand-diluted and mixed Fe-based oxygen carriers with potassium salts. *Fuel* **2023**, *339*, No. 127372.

(12) Störner, F.; Knutsson, P.; Leion, H.; Mattisson, T.; Rydén, M. An improved method for feeding ash model compounds to a bubbling fluidized bed − CLC experiments with ilmenite, methane, and K2CO3. *Greenhouse Gases: Sci. Technol.* **2023**, *13*, 546−564, DOI: 10.1002/ghg.2218.

(13) Lu, D. Y.; Tan, Y.; Duchesne, M. A.; McCalden, D. Potassium capture by ilmenite ore as the bed material during fluidized bed conversion. *Fuel* **2023**, *335*, No. 127008.

(14) Hildor, F.; Zevenhoven, M.; Brink, A.; Hupa, L.; Leion, H. Understanding the Interaction of Potassium Salts with an Ilmenite Oxygen Carrier Under Dry and Wet Conditions. *ACS Omega* **2020**, *5*, 22966−22977.

(15) Brorsson, J.; Staničić, I.; Gastaldi, J.; Mattison, T.; Hellman, A. Thermodynamic properties for metal oxides from first-principles. *Comput. Mater. Sci.* **2024**, *233*, No. 112690.

(16) Staničić, I.; Brorsson, J.; Hellman, A.; Mattisson, T.; Backman, R. Thermodynamic Analysis on the Fate of Ash Elements in Chemical Looping Combustion of Solid Fuels—Iron-Based Oxygen Carriers. *Energy Fuels* **2022**, *36*, 9648−9659.

(17) den Hoed, P.; Luckos, A. Oxidation and Reduction of Iron-Titanium Oxides in Chemical Looping Combustion: A Phase-Chemical Description. *Oil Gas Sci. Technol. − Rev. d'IFP Energies Nouv.* **2011**, *66*, 249−263.

(18) Chen, L.; Liu, D.; Xue, J.; Sun, Z.; Shen, L. Mechanism of phase segregation in ilmenite oxygen carriers for chemical-looping combustion. *Chem. Eng. J.* **2024**, *479*, No. 147921.

(19) Gyllén, A.; Knutsson, P.; Lind, F.; Thunman, H. Magnetic separation of ilmenite used as oxygen carrier during combustion of biomass and the effect of ash layer buildup on its activity and mechanical strength. *Fuel* **2020**, *269*, No. 117470.

(20) Bale, C. W.; Bélisle, E.; Chartrand, P.; Decterov, S. A.; Eriksson, G.; Gheribi, A. E.; Hack, K.; Jung, I.-H.; Kang, Y.-B.; Melançon, J.; et al. FactSage thermochemical software and databases, 2010−2016. *Calphad* **2016**, *54*, 35−53.

(21) Brorsson, J.; Staničić, I.; Gastaldi, J.; Mattison, T.; Hellman, A. Thermodynamic properties for metal oxides from first-principles. *Comput. Mater. Sci.* **2024**, *233*, No. 112690, DOI: 10.1016/j.commatsci.2023.112690.

(22) Benisek, A.; Dachs, E. The accuracy of standard enthalpies and entropies for phases of petrological interest derived from density-functional calculations. *Contrib. Mineral. Petrol.* **2018**, *173*, No. 90, DOI: 10.1007/s00410-018-1514-x.

(23) Lattard, D. Experimental evidence for the exsolution of ilmenite from titaniferous spinel. *Am. Mineral.* **1995**, *80*, 968−981.

(24) Corcoran, A.; Knutsson, P.; Lind, F.; Thunman, H. Comparing the structural development of sand and rock ilmenite during long-term exposure in a biomass fired 12 MWth CFB-boiler. *Fuel Process. Technol.* **2018**, *171*, 39−44.